



## Article

# Comparative Analysis of Climate Change Impacts on Climatic Variables and Reference Evapotranspiration in Tunisian Semi-Arid Region

Basma Latrech <sup>1,\*</sup>, Taoufik Hermassi <sup>1,\*</sup> , Samir Yacoubi <sup>1</sup>, Adel Slatni <sup>1</sup>, Fathia Jarray <sup>1</sup> , Laurent Pouget <sup>2</sup> and Mohamed Ali Ben Abdallah <sup>1</sup>

<sup>1</sup> National Research Institute for Rural Engineering, Water and Forestry, University of Carthage, BPN 10, Ariana 2080, Tunisia; basma.latrech@gmail.com (B.L.); samir.yacoubi@ingref.ucar.tn (S.Y.); slatni.adel@gmail.com (A.S.); fathiajarray1993@gmail.com (F.J.); benabdallah\_medali@yahoo.fr (M.A.B.A.)

<sup>2</sup> Water Technological Center, CETAQUA, Ctra. d'Esplugues, 75, Cornellà de Llobregat, 08940 Barcelona, Spain; laurent.pouget@cetaqua.com

\* Correspondence: taoufik.hermassi@ingref.ucar.tn

**Abstract:** Systematic biases in general circulation models (GCM) and regional climate models (RCM) impede their direct use in climate change impact research. Hence, the bias correction of GCM-RCMs outputs is a primary step in such studies. This study compares the potential of two bias correction methods (the method from the third phase of the Inter-Sectoral Impact Model Intercomparison Project (ISIMIP3) and Detrended Quantile Matching (DQM)) applied to the raw outputs of daily data of minimum and maximum air temperatures and precipitation, in the Cap-Bon region, from eight GCM-RCM combinations. The outputs of GCM/RCM combinations were acquired from the European branch of the coordinated regional climate downscaling experiment (EURO-CORDEX) dataset for historical periods and under two representative concentration pathway (RCP4.5 and RCP8.5) scenarios. Furthermore, the best combination of bias correction/GCM-RCM was used to assess the impact of climate change on reference evapotranspiration ( $ET_0$ ). Numerous statistical indicators were considered to evaluate the performance of the bias correction/historical GCM-RCMs compared to the observed data. Trends of the Hargreaves–Samani  $ET_0$  model during the historical and projected periods were determined using the TFPMK method. A comparison of the bias correction methods revealed that, for all the studied model combinations, ISIMIP3 performs better in reducing biases in monthly precipitation. However, for  $T_{max}$  and  $T_{min}$ , the biases are greatly removed when the DQM bias correction method is applied. In general, better results were obtained when the HadCCLM model was used. Before applying bias correction, the set of used GCM-RCMs projected reductions in precipitation for most of the months compared to the reference period (1982–2006). However,  $T_{min}$  and  $T_{max}$  are expected to increase in all months and for the three studied periods. Hargreaves–Samani  $ET_0$  values obtained from the best combination (DQM/HadCCLM) show that RCP8.5 (2075–2098) will exhibit the highest annual  $ET_0$  increase compared to the RCP4.5 scenario and the other periods, with a change rate equal to 11.85% compared to the historical period. Regarding spring and summer seasons, the change rates of  $ET_0$  are expected to reach 10.44 and 18.07%, respectively, under RCP8.5 (2075–2098). This study shows that the model can be used to determine long-term trends in  $ET_0$  patterns for diverse purposes, such as water resources planning, agricultural crop management and irrigation scheduling in the Cap-Bon region.

**Keywords:** bias correction; GCM/RCMs combinations; reference evapotranspiration; Cap-Bon



**Citation:** Latrech, B.; Hermassi, T.; Yacoubi, S.; Slatni, A.; Jarray, F.; Pouget, L.; Ben Abdallah, M.A. Comparative Analysis of Climate Change Impacts on Climatic Variables and Reference Evapotranspiration in Tunisian Semi-Arid Region. *Agriculture* **2024**, *14*, 160. <https://doi.org/10.3390/agriculture14010160>

Academic Editor: Ningbo Cui

Received: 25 October 2023

Revised: 20 November 2023

Accepted: 23 November 2023

Published: 22 January 2024



**Copyright:** © 2024 by the authors. Licensee MDPI, Basel, Switzerland. This article is an open access article distributed under the terms and conditions of the Creative Commons Attribution (CC BY) license (<https://creativecommons.org/licenses/by/4.0/>).

## 1. Introduction

Climate change is one of the most pressing environmental issues of the 21st century [1]. Therefore, the assessment and prediction of potential impacts of climate change and mitigation at global and regional scales have become a challenge for scientists, decision-makers,

and stakeholders. Global climate models (GCMs), as sources for generating present and future climate data, have been extensively adopted for climate-change-related studies [2]. However, simulated GCMs outputs are of high spatial resolution (larger than 50 km) and involve large biases relative to the observed data, which impede their use in local and regional impact studies [3,4]. To overcome this shortcoming, downscaling of the raw GCM outputs using statistical or dynamical techniques is widely adopted by researchers. The statistical downscaling approach involves the use of different techniques to establish a relationship between large-scale climate patterns and regional scale observed climate time series [5]. Dynamic downscaling approaches consist of running a climate model at a finer resolution, referred to as regional climate models (RCMs), using the coarse outputs of a GCM [6].

Despite their satisfactory resolution for hydro-climatological studies, historical RCMs output biases are still evident when compared to observed climate data. These errors are generally the results of imperfect conceptualization, discretization, and spatial averaging within grids [7]. Thus, additional post-processing of RCMs predictions before use is required [8]. To deal with this, a series of bias correction methods have been proposed, varying from scaling techniques to distribution mapping approaches. Corrections are mainly applied to the modeled mean, variance, and higher moments of a distribution. In addition, various techniques allowing for bias corrections to all quantiles were developed [9]. Different studies assessed the potential of numerous bias adjustment methods in removing biases in GCMs and RCMs. Casanueva et al. [10] compared eight bias adjustment methods and concluded that trend-preserving methods are suitable for post-processing model outputs since they allow for biases to be minimized while keeping the raw original climate change signal. Themeßl et al. [11] showed that quantile mapping methods performed better in the correction of raw RCMs outputs. However, bias adjustment techniques present some limitations and uncertainties related to the uncertainty of observational reference data and resolution mismatches [10].

In Mediterranean areas, water resources are being severely threatened by overexploitation. In the Maghreb countries, including Tunisia, as well as in some sectors of northern Mediterranean countries, the situation could become more relevant since current imbalances between water supply and demand are accentuated by the consequences of climate change [12]. In this context, good knowledge of the hydrological terms is needed to ensure the sustainable use of water resources. Reference evapotranspiration ( $ET_0$ ), as the essential component of the hydrological cycle, is the major cause of water losses from the earth. Thus, appropriate estimation of  $ET_0$  is of vital importance in climatological and hydrological studies, and agricultural water resources management. It is a key input in hydrological modeling, irrigation planning and management, the estimation of crop water requirements, agricultural drought monitoring, climate change, and water conservation modelling [13,14]. Since the agriculture sector is the largest consumer of the available freshwater resources in Tunisia, consuming more than 75% [15], understanding the relationship between climate environment and evapotranspiration is a fundamental requirement to estimate the depth of required water to achieve optimal agricultural production [16]. As one of the most important agricultural hubs of Tunisia, the Cap-Bon region produces the majority of the nation's exported crops and significantly participates in the creation of employment, contributing to food security for both the local and national communities [15]. Due to the expansion of irrigated areas in this region, water resources, already overexploited, are subjected to a significant demand pressure, leading to the depletion of groundwater resources and a deterioration in their quality. These critical conditions have led to severe environmental and social issues among users [17]. In the context of climate change, the efforts made by the state to mitigate water scarcity in the Cap-Bon (supply water via canal from Medjerda, providing up to 60% subsidies to farmers who invest in water-saving irrigation technologies, etc.), are insufficient. Hence, more planned scenarios for the irrigation of water and adaptations to decision-making rules should be applied. Due to the impact of climate change, changes in the meteorological variables will result in a change in the  $ET_0$  pattern. It is noteworthy to

point out that RCMs do not incorporate  $ET_0$  values; therefore, these need to be computed separately. Changes in  $ET_0$  will affect the availability, sustainability, and management of water resources. Therefore, ensuring better assessment of agricultural water demand requires a good understanding of historical and future changes in  $ET_0$  trends [18,19].

During the recent few decades, different studies have investigated the effects of climate change on reference evapotranspiration. Tabari et al. [20], revealed that  $ET_0$  presents a tendency to increase significantly in most climatic stations in Iran. In addition, Rahman et al. [21] examined the actual and projected trends of  $ET_0$  in Bangladesh. The authors used 39 years of past and downscaled CMIP5 daily meteorological data. The obtained results highlight that total  $ET_0$  values are expected to highly increase under the RCP8.5 scenario compared to historical and RCP4.5 scenarios. Furthermore, Chaouche et al. [22] studied the spatial distribution and temporal pattern of  $ET_0$  for a Mediterranean climate area in France. Their results indicated increasing trends in annual  $ET_0$  throughout the study area. Yassen et al. [23], investigated the spatiotemporal changes in annual and monthly  $ET_0$  in Egypt. They found a statistically significant change in annual  $ET_0$  in the Nile region.

To our knowledge, studies focusing on the identification of adequate GCM-RCMs for generating present and future climate data for Tunisia, in particular for the Cap-Bon region, are still limited or non-existent. This impedes the correct prediction of  $ET_0$  behavior and could lead to the future mismanagement of water resources, particularly in the irrigated agricultural sector. To overcome these limitations, this paper investigates the accuracy of bias-corrected GCM-RCMs in reproducing climate variables for impact studies. Thus, the specific objectives of this study are to: (1) explore the performances of two bias-corrected methods (ISIMIP3 and Detrended Quantile Matching) in post-processing GCM-RCMs outputs; in particular precipitation and air temperature; and (2) assess the climate change impacts on the reference evapotranspiration under RCP4.5 and RCP8.5 scenarios.

## 2. Data and Methods

### 2.1. Data Collection

The minimum and maximum air temperatures and precipitation at a daily time-scale were acquired for the period 1982–2020 from the National Meteorological Institute. Although the overall quality of the used dataset is good, some of the missing data were substituted with the corresponding average value of other years. The collected database was uploaded to the Climadjust platform [24,25], a web service (<https://climadjust.com/>; accessed on 1 February 2023) created with the support of the Copernicus Climate Change Service, to generate bias-corrected climate model simulations from the ensembles of the Coupled Model Intercomparison Project (CMIP) and Coordinated Regional Climate Downscaling Experiment (CORDEX) datasets or customized areas of interest. In the present study, we refer to the CORDEX domain centered on the Euro-Mediterranean area, known as EURO-CORDEX. Climate projections were provided using different combinations of general circulation models (GCMs) and regional climate models (RCMs) with different grid resolutions. GCMs have a 100–500 km horizontal resolution [26]. RCMs simulate the climate for a limited region by being constrained with boundary conditions from a global simulation by “downscaling”. Climate simulation data acquired from the EURO-CORDEX initiative are focused on grid sizes of 12.5 km (EUR-11 grid) [27]. Future climate projections were modeled under two different representative concentration pathways (RCPs) for greenhouse gas scenarios (RCP 4.5 and RCP 8.5).

Daily minimum and maximum air temperatures and precipitation from eight climate model combinations, between six GCMs (MOHC-HadGEM2-ES, MPI-M-MPI-ESM-LR, CNRM-CERFACS-CNRM-CM5, ICHEC-EC-EARTH, IPSL-IPSL-CM5A-MR, NCC-NorESM1-M) and six RCMs (CCLM4-8-17, REMO2009, RACMO22E, RCA4, HIRHAM5, REMO2015), as described in Table 1, were used in this study.

**Table 1.** Climate model combinations used for daily precipitation and temperature projections.

GCM	RCM	Acronym
MOHC-HadGEM2-ES	CCLM4-8-17	HadCCLM
MPI-M-MPI-ESM-LR	REMO2009	MPIREMO <sub>r2</sub>
MPI-M-MPI-ESM-LR	REMO2009	MPIREMO
CNRM-CERFACS-CNRM-CM5	RACMO22E	CM5RACM
ICHEC-EC-EARTH	RCA4	ECERCA4
MOHC-HadGEM2-ES	HIRHAM5	HadHIRH
IPSL-IPSL-CM5A-MR	RCA4	IPSRCA4
NCC-NorESM1	REMO2015	NorREMO15

## 2.2. Bias Correction Methods

Two bias correction (BC) methods (ISISMIP3 and detrended quantile matching) were selected among six different bias adjustment methods available in the Climadjust web service. Both methods were applied to the daily climate model outputs (precipitation, maximum and minimum air temperatures). These two methods were selected based on their distinct theoretical foundations: ISISMIP3 is parametric and the DQM method is empirical. Furthermore, these two BC methods are well-suited for climate data correction for agricultural impact assessment studies.

### 2.2.1. ISISMIP3

ISISMIP3 is a parametric quantile mapping bias adjustment technique developed for the third phase of ISIMIP. This method is suitable for different kinds of meteorological variables. It develops pseudo-future observations by transferring the simulated signals of each quantile to the historical observations. Furthermore, it considers the generated pseudo-future observations as a 'reference' to correct projections with parametric quantile mapping. This method is able to: (i) reduce biases in all percentiles of a distribution and (ii) proceed to time-series detrending and adding trends [28]. Values beyond thresholds are substituted by random values drawn from the adjusted marginal distribution [10]. The ISISMIP3 method generates bias-adjusted maximum and minimum air temperatures from bias-corrected amplitude and skewness of the diurnal temperature and daily mean temperature [28].

### 2.2.2. Detrended Quantile Matching

DQM is an empirical bias adjustment technique that consists of three phases, including: (i) deleting the long-term (linear) mean trend; (ii) applying empirical quantile mapping to the detrended series; and (iii) reapplying the mean trend to the corrected data. Then, the transfer function is calibrated using modelled and observed data. After the correction, precipitations below a specific wet-day threshold are registered as zero.

The climate change signal resulting from DQM will tend to align with the climate model under consideration, depending on the degree and the means of extrapolation required after the detrending step [29]. The climate change signal resulting from DQM will tend to match that of the climate model under consideration, depending on the degree and means of extrapolation still required after the trend suppression stage.

Using the DQM method, specific corrections for extremes are neglected, while the mean trend is preserved by construction [10]. The DQM algorithm can be defined as follows [30].

$$\hat{x}_{m,p}(t) = F_{o,h}^{-1} \left\{ F_{m,h} \left[ \frac{\bar{x}_{m,h} x_{m,p}(t)}{\bar{x}_{m,p}(t)} \right] \right\} \frac{\bar{x}_{m,p}(t)}{\bar{x}_{m,h}}$$

where  $\hat{x}_{m,p}(t)$  and  $x_{m,p}(t)$  are corrected and raw downscaled climate data at time  $t$  during a future period.  $F_{o,h}^{-1}$  and  $F_{m,h}$  are cumulative distribution functions (CDFs) of observed and simulated data during a historical period.  $\bar{x}_{m,p}(t)$  and  $\bar{x}_{m,h}$  are the long-term simulated mean over the historical and future periods.

### 2.3. Reference Evapotranspiration Estimations

Since projected climatic data is limited to minimum and maximum air temperatures, the Hargreaves–Samani (HgS) model was therefore selected to compute daily reference evapotranspiration ( $ET_0$ ) [31]. It is expressed as follows:

$$ET_0(\text{mm d}^{-1}) = 0.0135 \frac{Ra}{\lambda} \left( \frac{T_{\max} + T_{\min}}{2} + 17.8 \right) K_{rs} \sqrt{(T_{\max} - T_{\min})}$$

where 0.0135 is a factor for conversion from the American to the International System of Units.  $Ra$  is the extraterrestrial radiation ( $\text{MJ m}^{-2} \text{d}^{-1}$ ).  $\lambda$  is the latent heat of vaporization ( $\text{MJ kg}^{-1}$ ) for the mean air temperature  $T$  ( $^{\circ}\text{C}$ ).  $K_{rs}$  is the radiation adjustment coefficient ( $^{\circ}\text{C}^{-0.5}$ ).

The HgS model is among the most extensively used temperature-based approaches due to its simplicity and reliability. In fact, the suitability of the HgS model has been widely assessed against the PM- $ET_0$  and grass lysimeter data, showing that the HgS model performs well in most climatic regions, except under a humid climate where a tendency to overestimate  $ET_0$  is registered [32]. Additionally, Sabziparvar and Tabari [33] evaluated the performances of three  $ET_0$  models, including the HgS, against the standard FAO56-PM model in eastern arid and semi-arid regions of Iran. The obtained results showed the superiority of the HgS model. Similarly, Jabloun and Sahli [34] assessed the HgS equation for computing daily  $ET_0$  against the FAO-56 PM method across Tunisian locations. The results indicated that the HgS model is adequate for Tunisian climatic conditions with a slight overestimation at inland sites, while a tendency towards underestimation is registered at coastal regions.

The Mann–Kendall (MK) is a non-parametric test generally used to detect trends (upward or downward) in a metrological variable time series. This test does not require normality or linearity to identify trends in a time series. Therefore, Yue et al. [35], have suggested the trend-free pre-whitened-MK test (TFPW-MK test) which is applied to remove the influence of autocorrelation on the MK. The Sen's slope estimator [36,37] is used to estimate the magnitude of the linear trend slope in the  $ET_0$  time series. Both tests were applied in this study for reference evapotranspiration trend detection. Details on the TFPW-MK test and Sen's slope estimator are described in Latrech et al. [38].

### 2.4. Performance Metrics

Bias correction methods and model performances in reproducing the observed climatic data were assessed through the Taylor diagram [39], which considers three performance evaluation criteria: the linear correlation coefficient ( $R$ ), standard deviation ( $\sigma$ ), and centered root mean square error (CRMSE). In order to strengthen the Taylor diagram, two additional evaluation indices, mean absolute error (MAE) and percent bias (PBIAS), were calculated. The assessment was made by comparing, separately, the raw and bias-corrected output of the historical simulations of each GCM-RCM model versus the reference datasets (1982–2005). According to Gado et al. [40] the best-classified bias correction technique during the historical period allows for the best performance for the projected conditions to be reproduced.



$$R = \frac{\sum_{i=1}^N (x_i^o - \bar{x}_i^o)(x_i^m - \bar{x}_i^m)}{\sigma^o \sigma^m}$$

$$CRMSE = \left( \frac{1}{N} \sum_{i=1}^N [(x_i^o - \bar{x}_i^o)(x_i^m - \bar{x}_i^m)]^2 \right)^{0.5}$$

$$MAE = \frac{\sum_{i=1}^N |x_i^o - x_i^m|}{N}$$

$$PBIAS = \frac{\sum_{i=1}^N (x_i^m - x_i^o)}{\sum_{i=1}^N x_i^o} \times 100$$

where  $\sigma^o$  and  $\sigma^m$  are the standard deviations of the observed and simulated datasets, respectively. N is the number of the data. R-values can range from  $-1$  to  $+1$ . R values closer to  $-1$  and  $+1$  indicate high correlation between observed and modelled data. The lower the CRMSE, the more efficient the method and model accuracy. The optimal value of CRMSE is 0. The mean absolute error (MAE) shows the average model forecast error. Values of MAE vary from 0 to infinity [41]. The lower the value of MAE, the better the accordance. The percent bias (PBIAS) computes the average tendency of the modelled data to be greater or lower compared to their corresponding measured ones. The ideal value of PBIAS is 0. Positive values of PBIAS refer to an overestimation and vice versa.

### 3. Results and Discussion

#### 3.1. Performance of Bias Correction Methods

In addition to the statistical indicators, the Taylor diagrams for monthly precipitation, and maximum and minimum air temperatures were developed (Figures 1a and 2). The Taylor diagram is an effective method that displays a systematic and mathematical illustration of a model’s performance. In the diagram, the used models are shown with different markers, and bias correction methods are presented in different colors (red color: raw data; blue color: ISIMIP3 bias correction method; green color: DQM bias correction method).

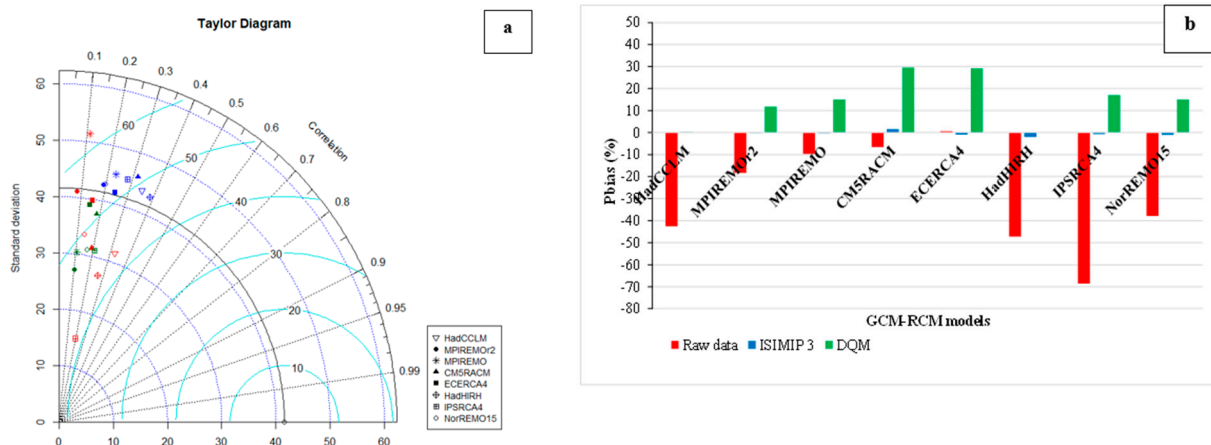


**Figure 1.** (a) Taylor diagram for comparison between the performances of bias correction methods and GCM-RCMs in reproducing monthly precipitation; and (b) percent bias in monthly precipitation with the two bias correction methods for all GCM-RCMs combinations.

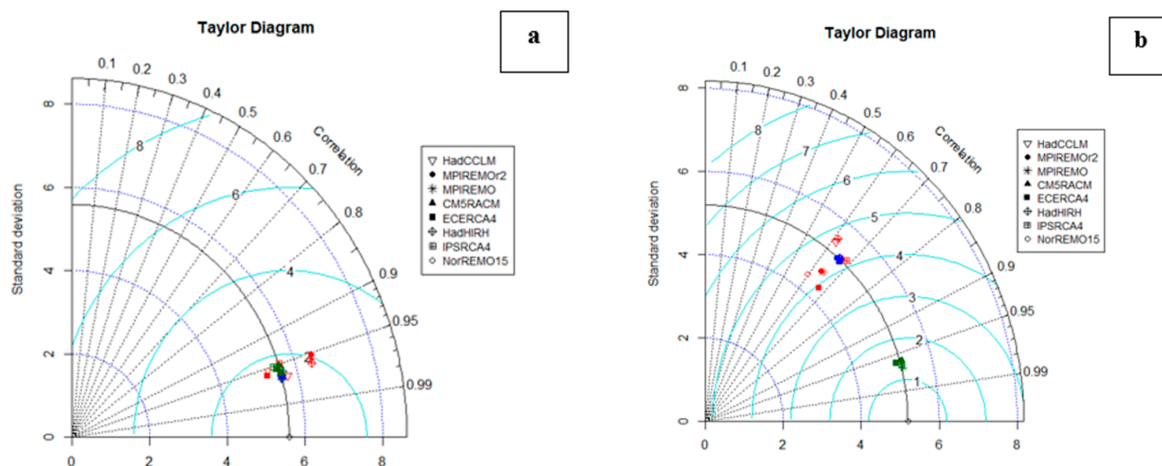


**Figure 2.** Taylor diagram for comparison between performances of GCM-RCM model outputs, after bias correction using two different methods, in reproducing monthly maximum (a); and minimum (b) air temperatures in the Cap-Bon region.

### 3.1.1. Precipitation

Figure 1a presents the performances of GCM-RCM models output, after bias correction using two different methods, in reproducing monthly precipitation in the Cap-Bon region. As shown in the Taylor diagram, the BC methods and models present different patterns. Regarding BC methods, ISIMIP3 performs better than the DQM method in reducing monthly precipitation bias for all the studied model combinations. Further analysis of the Taylor diagram shows that most of the bias-corrected data using the DQM method are worse than those obtained from the raw data. In the same context, Lange et al. [28], compared the performance of ISIMIP2b and ISIMIP3 bias correction methods in adjusting biases in climate model outputs. Their results revealed that, for all studied climate variables, the ISIMIP3 bias correction method performs better than the ISIMIP2b method in adjusting the bias for the majority of months and grid cells. In addition, Casanueva et al. [10], in an assessment of eight bias adjustment methods, found that the DQM shows a significant deviation from the raw trend for rainfall frequency. However, ISIMIP3 could preserve the model's raw signals for the different indices and variables. Therefore, the HadHIRH model using the ISIMIP3 bias correction method followed by the HadCCLM model yielded better results for monthly P estimations. Their corresponding R,  $\sigma$  criteria were improved compared to raw data. Nevertheless, the CRMSE was not significantly improved.

According to the PBIAS results (Figure 1b), the ISIMIP3 method performed well to reduce the gap between the corrected and observed data compared to the DQM method, with PBIAS values lower than 5%. However, the results of the MAE showed that application of any of the two bias correction methods worsened the results of the precipitation simulations even compared to the non-corrected data form.

### 3.1.2. Maximum and Minimum Air Temperature

Figure 2a presents the performances of GCM-RCM models outputs, after bias correction using ISIMIP3 and DQM methods, in reproducing monthly Tmax in the Cap-Bon region. The Taylor diagram reported that simulated data are highly correlated with the observations, with R values higher than 0.95 for all considered models and bias correction methods. Furthermore, obtained results emphasize that even raw data are able to well reproduce monthly Tmax.

Table 2 summarizes some statistical indicators estimated at a monthly scale. In general, both bias correction methods tend to decrease the raw model bias. Detailed analysis of the results (Table 2) highlights that, for all model combinations, comparable results are obtained when either ISIMIP or DQM bias correction method is used with a slightly higher

accuracy is accorded to ISIMIP3 method. Although the negligible differences in terms of performance, the best-performing models are HadCCLM and HadHIRH.

**Table 2.** Statistical indicators for comparison between measured and simulated mean monthly maximum and minimum air temperatures using eight GCM-RCM combinations.

Models	Tmax						Tmin					
	Raw Data		ISIMIP3		DQM		Raw Data		ISIMIP		DQM	
	PBIAS	MAE	PBIAS	MAE	PBIAS	MAE	PBIAS	MAE	PBIAS	MAE	PBIAS	MAE
HadCCLM	−6.35	1.65	0.04	1.09	0.03	1.09	8.44	4.06	0.20	3.41	0.06	1.13
MPIREMO <sub>r2</sub>	6.56	2.06	−0.03	1.17	0.13	1.42	−6.33	3.41	0.05	3.48	−0.08	1.16
MPIREMO	6.40	2.01	−0.03	1.16	0.07	1.39	−6.01	3.36	0.07	3.42	0.01	1.04
CM5RACM	−8.02	2.04	0.03	1.15	0.02	1.31	−20.32	4.11	0.09	3.43	−0.01	1.18
ECERCA4	−9.56	2.27	−0.04	1.19	−0.06	1.20	−21.29	4.03	0.08	3.36	−0.08	1.11
HadHIRH	0.88	1.55	0.04	1.08	0.10	1.29	2.18	3.80	0.34	3.42	0.03	1.08
IPSRCA4	−2.59	1.45	−0.05	1.19	0.05	1.35	−16.28	3.78	0.11	3.44	−0.08	1.09
NorREMO15	1.65	1.36	0.13	1.17	0.04	1.35	−0.68	3.53	0.25	3.38	−0.06	1.21

The potential of using bias correction methods to adjust the raw data of monthly Tmin generated from eight GCM-RCM model combinations was assessed using the Taylor diagram (Figure 2b) and some statistical descriptors (Table 2). As presented in Figure 2b, correlation coefficients determined for all studied corrected methods of Tmin model outputs using the ISIMIP3 method are of the same order of magnitude as those obtained for non-corrected forms. The R values range from 0.6 and 0.7. In addition, despite the clear reductions in PBIAS values, the MAE values were slightly improved compared to the non-corrected conditions. These results indicated that the ISIMIP3 bias correction method could not improve the Tmin models outputs. However, the DQM bias correction method allowed for satisfactory results of Tmin data to be obtained, with R values close to 0.95 for all GCM-RCM models. The PBIAS tended to 0 and MAE values varied from 1.04 to 1.21 °C/month for the MPIREMO and NorREMO15 models, respectively.

### 3.2. Projected Change of Meteorological Variables before Bias Correction

Precipitation, minimum and maximum air temperatures obtained from each GCM-RCM for the whole projected period, 2025–2098, were grouped into three time intervals (2025–2049, 2050–2074, 2075–2098). The change rates were determined compared to the reference period 1980–2005 (Figure 3).

Changes were assessed for each GCM-RCM output separately, before applying any bias correction method, compared to the reference period (1982–2005). To analyze the variation of climatic parameters, the precipitation variation was determined in terms of percentage, while the difference between the average temperature projected by the model and that recorded in the reference period was used for the air temperature. Monthly variability in the projected GCM-RCM outputs relative to P, Tmin and Tmax are shown in Figure 3. Regarding precipitation, the models predicted decreases, on average, for most of the months and in all three periods. Furthermore, a slight and partial increase was observed for January, February, and September, which are typically classified as rainy months in the Mediterranean climate. In addition, an increase in precipitation was observed in August, with 45% and 5% for both periods (2025–2049) and (2050–2074), respectively. Concerning minimum and maximum air temperatures, the change signal is clearer than that for precipitation. As shown in Figure 3, Tmin and Tmax are expected to increase in all months and for the three periods. In addition, obtained results highlight that the increment in air temperature is more pronounced in summer months (June, July and August) and moving in the future. Compared to a reference value of 31.4 °C, the Tmax variation in August varied from 0.86 to 1.9 °C in 2025–2049, from 1.1 to 2.7 °C in 2050–2074 and from 1.54 to 3.2 °C. For Tmin, the variation in August ranged from 1.2 to 1.9 °C in 2025–2049, from 1.7 to 2.8 °C in 2050–2074, and from 2.2 to 3.5 °C in 2074–2098.



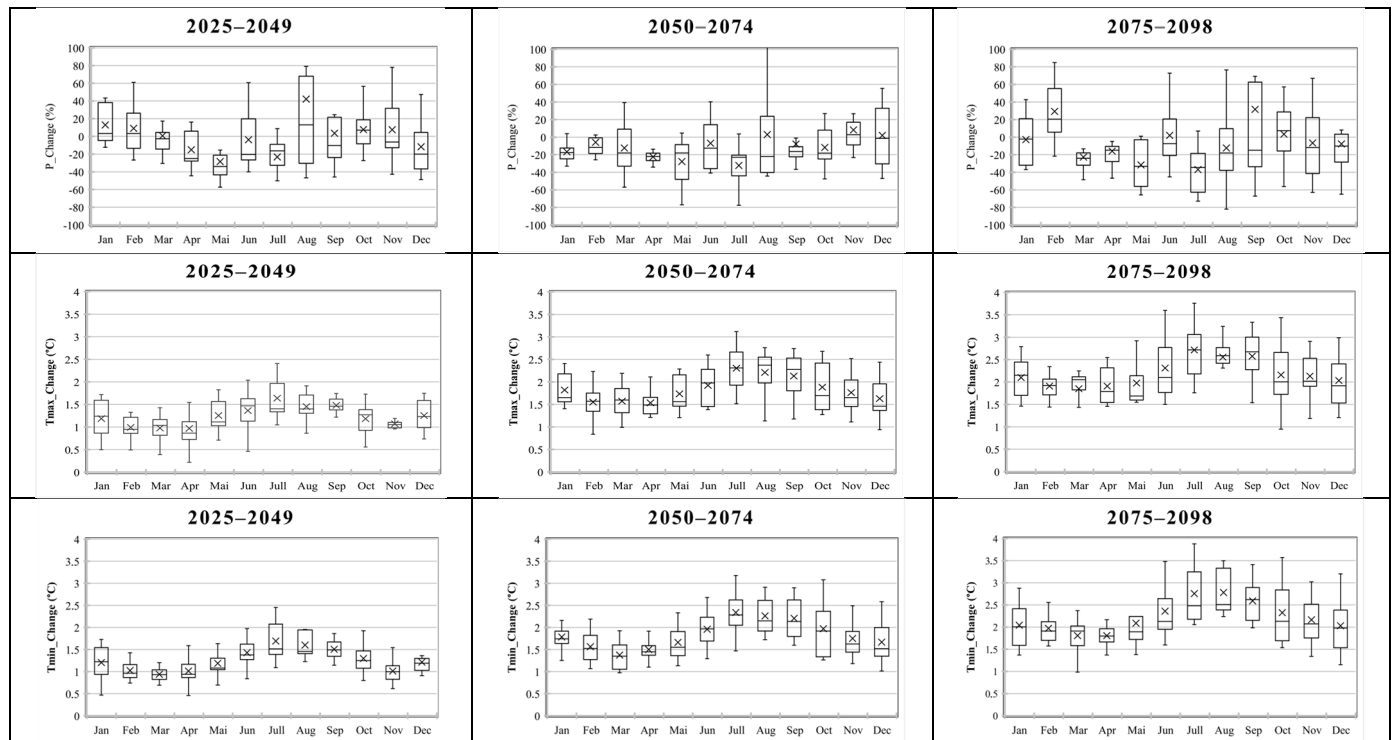


**Figure 3.** Boxplots representing the projected changes in mean monthly precipitation, minimum and maximum air temperature, and median values of the raw model outputs under the RCP4.5 scenario. The black horizontal line and the black cross show the models’ median and means, respectively.

3.3. Projected Changes in Bias-Corrected Tmax and Tmin under Both RCPs Scenarios

The DQM method was considered to correct the biases in predicted daily Tmin and Tmax under the two scenarios (RCP4.5 and RCP8.5). Then, the corrected data were gathered for three time periods (2025–2049), (2050–2074) and (2075–2098). The average monthly and annual change rates of the corrected HadCCLM Tmin and Tmax outputs, estimated separately for the three time periods, compared to the reference period (1982–2005) are shown in Table 3.

**Table 3.** Changes rate in yearly and monthly Tmax and Tmin for future periods.

	Tmax						Tmin					
	RCP4.5		RCP8.5		RCP4.5		RCP8.5		RCP4.5		RCP8.5	
	2025–2049	2050–2074	2075–2098	2025–2049	2050–2074	2075–2098	2025–2049	2050–2074	2075–2098	2025–2049	2050–2074	2075–2098
Annual	1.53	2.29	2.82	1.72	3.07	4.69	1.55	2.33	2.86	1.74	3.12	4.83
January	1.49	2.06	2.49	1.44	2.33	3.76	1.53	1.98	2.46	1.37	2.34	3.88
February	0.85	1.67	2.01	1.57	2.13	3.79	0.84	1.69	2.00	1.59	2.23	3.97
March	1.06	1.64	1.96	1.29	2.23	3.56	0.84	1.42	1.86	1.13	2.14	3.39
April	1.52	1.77	2.26	1.47	2.61	3.55	1.34	1.84	1.81	1.41	2.47	3.31
May	1.48	2.25	2.84	2.03	3.22	4.48	1.54	2.24	3.02	1.87	3.06	4.73
June	1.57	2.21	3.07	1.51	3.26	5.10	1.91	2.25	3.23	1.70	3.59	5.20
July	2.47	3.06	3.74	2.49	4.10	6.38	2.47	3.15	3.85	2.59	4.08	6.51
August	1.87	2.75	3.21	2.05	4.00	5.75	1.85	2.69	3.39	1.94	3.56	5.61
September	1.46	2.68	3.19	1.56	3.71	5.48	1.56	2.74	2.95	1.77	3.71	5.77
October	1.83	2.77	3.51	1.94	3.59	5.29	2.01	3.12	3.63	1.97	3.86	5.75
November	1.03	2.23	2.65	1.54	2.67	4.62	0.97	2.34	2.88	1.72	3.03	5.09
December	1.70	2.38	2.93	1.77	2.95	4.52	1.78	2.54	3.18	1.83	3.36	4.72

A clear increase is projected for both the monthly and annual Tmax and Tmin variables and for the three study periods. As expected, the increase is more pronounced under RCP 8.5 than under RCP4.5 and with moving into the future. Compared to the reference period (1982–2005), the change rates in annual average Tmax are estimated to 1.53, 2.29 and 2.82 °C under RCP4.5, respectively, for the (2025–2049), (2050–2074) and (2075–2098) periods. However, higher change rates are recorded under RCP 8.5, with values equal to 1.72, 3.07 and 4.69 °C, respectively, for the same periods. For the monthly time scale, the projected increases in Tmax vary from 0.85 to 2.47 °C, and from 1.96 to 3.74 °C during 2025–2049 and 2075–2098, respectively, under RCP4.5. In particular, the summer months exhibit the highest increase, with values projected up to 3.07, 3.74 and 3.21 in June, July and August under RCP4.5, while 5.10, 6.38 and 5.75 are expected under the RCP8.5 scenario.

Relatively comparable results were achieved by Senatore et al. [42], who assessed the effects of climate change on air temperature in the Mediterranean climate of southern Italy. The authors found that, regardless of the GCM-RCM model used, air temperature is expected to rise in all months as well as for the three studied periods. In addition, their results indicated that air temperature growth is faster in summer months and when moving into the future. Furthermore, Sellami et al. [43] used multi-model outputs from the EU-FP6 ENSEMBLES project to assess the hydrological responses of two Mediterranean catchments. Their results revealed that, in comparison to the reference period (1971–2000), monthly air temperatures tend to increase in the future scenario (2041–2071) in both catchments. Furthermore, the results showed that the increase in air temperature is higher in summer months than in winter.

Compared to the reference period, the annual average growth rates of Tmin rise by 1.55, 2.33, and 2.86 °C under RCP4.5 and by 1.74, 3.12 and 4.83 °C under RCP8.5, respectively, for the (2025–2049), (2050–2074) and (2075–2098) periods. Our results are slightly higher than those obtained by Sundaram and Radhakrishnan [44] in the Thanjavur district. The authors found that annual Tmin is projected to increase by about 1.06–2.32 °C under the RCP4.5 scenario, and by 1.59–3.87 °C under the RCP8.5 scenario for short and long-term scenarios.

Regarding monthly Tmin, positive change rates were recorded for all months and study periods compared to the reference period. In particular, March exhibited the lowest increase for all periods and under both scenarios. However, July was projected to experience the highest increase for all study periods and scenarios. As shown in Table 3, overall, annual, and monthly Tmin increase at a higher rate than Tmax. In this context, Tabari and Hosseinzadeh Talaee [45], examined the trends of Tmax and Tmin at different time scales in Iran. Their results show an upward trend for both variables, and that Tmin increases faster than Tmax in most months and seasons.

### 3.4. Temporal Changes in $ET_0$ under Both RCP Scenarios

In this study, the Tmax and Tmin outputs of the HadCCLM model, corrected using the DQM method, were considered to estimate daily  $HgS_{ET_0}$ . The calculation was made for historical and future periods under RCP4.5 and RCP8.5 scenarios. For the historical period (1982–2006), the obtained values were aggregated to monthly data and compared to their corresponding  $HgS_{ET_0}$ , and calculated using the observed Tmin and Tmax. Results of the comparison show that simulated monthly  $HgS_{ET_0}$  highly approximate the results obtained using measured Tmin, and Tmax with slope of regression line and  $R^2$  values equal to 1 and 0.95, respectively. A further assessment demonstrated the accuracy of the HadCCLM outputs in estimating  $HgS_{ET_0}$ , with RMSE = 10.12 mm month<sup>-1</sup>, MAE = 6.73 mm month<sup>-1</sup> and PBIAS = 0.25%. Furthermore, daily  $HgS_{ET_0}$  data were aggregated to a yearly scale, as shown in Figure 4. Results of the change rates of projected annual and seasonal  $ET_0$  under the RCP 4.5 and 8.5 scenarios, compared to the historical period, are presented in Table 4.

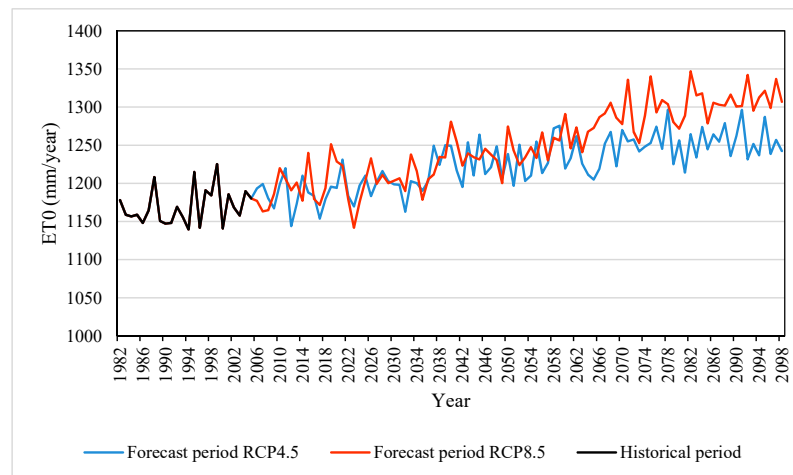


**Figure 4.** Patterns of annual  $ET_0$  for historical and RCP scenarios.

During the historical period (1982–2006), annual  $HgS\_ET_0$  values varied between 1140 and 1230 mm, with a slight tendency to increase during that period. In addition, an  $ET_0$  increase was projected for most studied periods. It is evident that the RCP8.5 will experience a higher annual  $ET_0$  increase compared to the RCP4.5 scenario because of the different greenhouse gas concentrations for the RCP [46]. Under the RCP4.5 scenario, the average annual  $ET_0$  is expected to reach 1214.81, 1237.2, and 1254.88 mm for the periods 2025–2049, 2050–2074 and 2075–2098, respectively. Relative to the historical period, these values correspond to change rates of about 4, 5.8 and 7.3%. However, under RCP 8.5, the change rates of annual  $ET_0$  are evaluated to 4.5, 8.3 and 11.8%, respectively, for the same periods.

In the Nabeul region, irrigation water requirements present a large interannual variability, with the highest water demand for summer and spring seasons. For this reason, when considering seasonal scale, the future change in  $ET_0$  will be assessed only for summer and spring. For these two seasons, increases in  $ET_0$  are expected in the future for both scenarios (RCP4.5 and RCP8.5), where the severity of the increase depends on the emissions scenario. As summarized in Table 4, during spring and summer seasons, the accumulated  $ET_0$  would reach 334 and 501 mm, respectively, for the period 2075–2098, under RCP 4.5. However, higher values are registered for RCP8.5. Compared to the historical period, these increments correspond to a change rate of 10.44 and 18.07%, respectively, for the spring and summer seasons.

**Table 4.** Change rates of historical and projected seasonal and annual  $ET_0$ .

	Historical		RCP4.5		RCP8.5		
	1982–2006	2025–2049	2050–2074	2075–2098	2025–2049	2050–2074	2075–2098
<b>Annual</b>							
$ET_0$ (mm)	1169.20	1214.81	1237.20	1254.88	1221.60	1266.04	1307.73
Change (mm)		45.61	68.00	85.68	52.40	96.84	138.53
Change (%)		3.90	5.82	7.33	4.48	8.28	11.85
<b>Spring season</b>							
$ET_0$ (mm)	310.95	324.89	327.80	334.03	351.68	337.63	345.82
Change (mm)		13.94	16.85	23.07	40.73	26.67	34.87
Change (%)		4.17	5.04	6.91	12.19	7.99	10.44
<b>Summer season</b>							
$ET_0$ (mm)	470.24	488.09	498.28	501.67	490.77	510.63	530.59
Change (mm)		17.85	28.04	31.43	20.53	40.39	60.35
Change (%)		5.34	8.39	9.41	6.15	12.09	18.07

Table 5 summarizes the results of TFPWMK Z-values, trend Sen’s slopes for annual, seasonal (spring and summer), and monthly ET<sub>0</sub>. Sen’s slopes of significant trends (95% levels) are shown in bold character. During the historical period (1982–2006), the increase of annual ET<sub>0</sub> was insignificant, with a Sen’s slope value close to 1 mm year<sup>-1</sup>. Under the RCP4.5 scenario, annual ET<sub>0</sub> upward trends were estimated as 1.41 and 1.49 mm year<sup>-1</sup> for 2025–2049 and 2050–2074, respectively, while an insignificant decreasing trend was recorded for the period 2075–2098. For the same periods, the annual ET<sub>0</sub> increases under the RCP 8.5 scenario were estimated at 1.56, 2.7 and 0.81 mm year<sup>-1</sup>, respectively, proving that the ET<sub>0</sub> increases faster with increasing radiative forcing levels. During the historical period, spring and summer seasonal ET<sub>0</sub> (dry seasons) tend to increase, with Sens’s slope values equal to 0.79 and 0.29, respectively.

During 2050–2075, ET<sub>0</sub> values registered in the summer season presented a non-significant decrease under RCP 4.5. While a non-significant mix of trends was recorded under the RCP4.5 scenario for the three studied periods, a significant increasing trend at a level of 0.05 was observed for the two dry seasons under the RCP8.5 scenario, except for the 2075–2098 time period. Comparable results were achieved by Zhao et al. [47], who investigated trends in annual and seasonal ET<sub>0</sub> in different agricultural areas and the whole country of China under four RCP scenarios. They revealed the existence of a positive correlation between the ET<sub>0</sub> growth rate and radiative forcing.

The intersection of the two curves of annual ET<sub>0</sub> (Figure 4), particularly during the period 2025–2049, was justified by the comparable Sen’s slope values under both RCP scenarios. Nevertheless, the period 2075–2098 exhibited the largest difference in terms of annual ET<sub>0</sub> patterns, accentuated by the insignificant decline under the RCP4.5 scenario.

Table 5. TFPWMK statistics and Sen’s slope values for multi-scale ET<sub>0</sub> under different scenarios.

	Historical Period		RCP 4.5						RCP 8.5					
	1982–2006		2025–2049		2050–2074		2075–2098		2025–2049		2050–2074		2075–2098	
	MK Z-Value	Sen’s Slope	MK Z-Value	Sen’s Slope	MK Z-Value	Sen’s Slope	MK Z-Value	Sen’s Slope	MK Z-Value	Sen’s Slope	MK Z-Value	Sen’s Slope	MK Z-Value	Sen’s Slope
Annual	1.48	1.01	2.55	<b>1.41</b>	1.71	1.49	-0.37	-0.23	2.06	<b>1.56</b>	3.54	<b>2.7</b>	1.16	0.81
Spring	3.17	<b>0.79</b>	1.9	0.64	1.58	0.65	0.63	0.25	2.69	<b>0.91</b>	2.96	<b>1.02</b>	0.26	0.15
Summer	0.58	0.29	2.64	<b>1.32</b>	-0.21	-0.16	0.05	0.10	2.22	<b>1.29</b>	2.01	<b>1.15</b>	2.27	0.96
January	1.80	0.14	-0.32	-0.02	1.90	<b>0.12</b>	-0.68	-0.05	0.22	0.018	0.025	0.002	0.1	0.01
February	0.53	0.04	0.62	0.04	1.81	0.13	0.10	0.02	1.04	0.14	0.17	0.02	-2.16	<b>-0.25</b>
March	0.90	0.16	1.86	0.19	1.56	0.22	-0.32	-0.04	2.5	<b>0.3</b>	2.65	<b>0.35</b>	0	0.008
April	3.43	<b>0.48</b>	1.36	0.21	0.62	0.15	-0.05	-0.04	0.96	0.28	1.01	0.2	-0.21	-0.06
May	0.05	0.01	0.12	0.05	1.26	0.34	0.69	0.18	1.51	0.27	1.61	0.37	0.95	0.3
June	-0.80	-0.14	1.21	0.33	-0.37	-0.08	0.32	0.08	1.46	0.39	1.86	0.4	2.27	0.73
July	1.27	0.38	2.80	<b>0.57</b>	-0.71	-0.25	0.37	0.15	0.47	0.09	-0.27	-0.08	0.63	<b>0.14</b>
August	0.53	0.15	1.16	0.26	0.02	0.01	-0.89	-0.26	-0.22	-0.05	2.75	<b>0.78</b>	0.89	0.28
September	0.30	0.10	1.56	0.29	3.20	<b>0.63</b>	-0.63	-0.05	-0.17	-0.02	1.31	0.27	0.05	0.01
October	-0.60	-0.09	0.03	0.01	0.32	0.04	0.58	0.07	0.77	0.099	-0.07	-0.01	-1.26	-0.17
November	0.10	0.02	0.07	0.01	1.86	0.12	-0.42	-0.04	0.57	0.03	0.27	0.02	-0.15	-0.008
December	-1.16	-0.02	-0.76	-0.03	1.86	0.09	-0.73	-0.04	0.91	0.07	0.47	0.03	1	0.05

Significant trends (95% levels) are shown in bold character.

The trends of monthly ET<sub>0</sub> using Sen’s slope estimator and TFPW-MK in the historical period, RCP4.5 and RCP8.5 scenarios are also shown in Table 5. During 1982–2006, monthly ET<sub>0</sub> presented a mix of non-significant tendencies. However, a significant upward trend was detected (*p*-value = 0.05) in April, with a Sen’s slope equal to 0.48 mm year<sup>-1</sup>. Relatively similar behavior was observed in overall projected data for both RCPs. In particular, under RCP4.5, our results tended to generalize the decrease in ET<sub>0</sub> for most months in 2075–2098. This might be explained by the fact that T<sub>min</sub> tends to increase faster than T<sub>max</sub>, which would decrease ΔT (T<sub>max</sub> – T<sub>min</sub>).

#### 4. Conclusions

Despite the existence of advanced regional climate models (RCMs), bias correction is still commonly considered a primordial step within climate impact studies to remove the systematic deviations of climate model outputs. Based on diagrams and statistical indicators, it can be concluded that, for the removal of bias from simulated precipitation, the ISIMIP3 bias correction method performs better than the DQM method. However, DQM was found to be more effective for T<sub>min</sub> and T<sub>max</sub>. Regarding GCM-RCM accuracy, the HadCCLM, followed by the HadHIRH model, proved to be the best combinations for generating precipitation and minimum and maximum air temperatures.

For both RCP scenarios, the HadCCLM model projects a clear increase in monthly and annual T<sub>max</sub> and T<sub>min</sub> for the three study periods. Furthermore, the increase is more important under the RCP 8.5 scenario than that under the RCP4.5 and moving into the future. As expected, annual HgS\_ ET<sub>0</sub> amounts are projected to increase under both RCP scenarios. Compared to historical data, the highest change rates were recorded during the period 2075–2098, with values equal to 7.3 and 11.8%, respectively, under RCP4.5 and RCP8.5. According to the TFPWMK test, the annual ET<sub>0</sub> tends to increase with Sen's slope values equal to 1.41 and 1.49 mm year<sup>-1</sup> for 2025–2049 and 2050–2074 under the RCP4.5 scenario. Our results also highlight that ET<sub>0</sub> tends to increase more quickly with increasing radiative forcing levels, reaching 2.7 mm year<sup>-1</sup> for the period 2050–2074 under RCP8.5. Relatively similar ET<sub>0</sub> behavior was observed for spring and summer seasons, where, change rates of 6.9 and 9.41% were recorded for RCP4.5, and 10.44 and 18.07% were recorded for RCP8.5.

It should be pointed out that, in our context of water resources scarcity, the projected increase in ET<sub>0</sub> would amplify the already existing problems i.e., over-withdrawals of groundwater, increasing water expenditure cost and energy consumption, food insecurity, increasing soil salinity, etc. Therefore, our findings will, as a tool, provide support for hydrological modeling, irrigation scheduling, water resources planning and agricultural crop management in determining adaptive appropriate measures to combat climate change.

**Author Contributions:** Conceptualization, B.L., T.H. and S.Y.; methodology, B.L., T.H. and S.Y.; software, B.L.; validation, T.H. and S.Y.; formal analysis, B.L.; data curation, B.L.; writing—original draft preparation, B.L.; writing—review and editing, T.H., S.Y., A.S., F.J., L.P. and M.A.B.A.; supervision, T.H. and S.Y. All authors have read and agreed to the published version of the manuscript.

**Funding:** This research was funded by MAGO project through PRIMA program supported by the European Union. The grant agreement number 2022. The APC was funded by PROJET MAGO/INRGREF. The authors are grateful to the MAGO project for funding this research.

**Data Availability Statement:** The data cannot be shared because they are a priority of INRGREF.

**Acknowledgments:** Thanks are due to the National Research Institute for Rural Engineering, Water and Forestry (INRGREF) for the valuable support of this research.

**Conflicts of Interest:** The authors declare no conflict of interest.

#### References

1. Vaghefi, S.A.; Abbaspour, N.; Kamali, B.; Abbaspour, K.C. A toolkit for climate change analysis and pattern recognition for extreme weather conditions e Case study: California-Baja California Peninsula. *Environ. Model. Softw.* **2017**, *96*, 181–198. [[CrossRef](#)]
2. Zolghadr-Asli, B.; Bozorg-Haddad, O.; Sarzaeim, P.; Chu, X. Investigating the variability of GCMs' simulations using time series analysis. *J. Water Clim. Change* **2018**, *10*, 449–463. [[CrossRef](#)]
3. Sillmann, J.; Kharin, V.; Zhang, X.; Zwiers, F.; Bronaugh, D. Climate extremes indices in the CMIP5 multimodel ensemble: Part 1. Model evaluation in the present climate. *J. Geophys. Res. Atmos.* **2013**, *118*, 1716–1733. [[CrossRef](#)]
4. Hostetler, S.W.; Alder, J.R.; Allan, A.M. *Dynamically Downscaled Climate Simulations over North America: Methods, Evaluation and Supporting Documentation for Users*; U.S. Geological Survey Open-File Report 2011-1238; U.S. Geological Survey: Menlo Park, CA, USA, 2011; 64p.
5. Dibike, Y.B.; Coulibaly, P. Hydrologic impact of climate change in the Saguenay watershed: Comparison of downscaling methods and hydrologic models. *J. Hydrol.* **2005**, *307*, 145–163. [[CrossRef](#)]



6. Ahmed, K.F.; Wang, G.L.; Silander, J.; Wilson, A.M.; Allen, J.M.; Horton, R.; Anyah, R. Statistical downscaling and bias correction of climate model outputs for climate change impact assessment in the US northeast. *Glob. Planet. Change* **2013**, *100*, 320–332. [[CrossRef](#)]
7. Teutschbein, C.; Seibert, J. Bias correction of regional climate model simulations for hydrological climate-change impact studies: Review and evaluation of different methods. *J. Hydrol.* **2012**, *456*, 12–29. [[CrossRef](#)]
8. Enayati, M.; Bozorg-Haddad, O.; Bazrafshan, J.; Hejabi, S.; Chu, X. Bias correction capabilities of quantile mapping methods for rainfall and temperature variables. *J. Water Clim. Change* **2021**, *12*, 401–419. [[CrossRef](#)]
9. Gudmundsson, L.; Bremnes, J.B.; Haugen, J.E.; Engen-Skaugen, T. Technical Note: Downscaling RCM precipitation to the station scale using statistical transformations—A comparison of methods. *Hydrol. Earth Syst. Sci.* **2012**, *16*, 3383–3390. [[CrossRef](#)]
10. Casanueva, A.; Herrera, S.; Iturbide, M.; Lange, S.; Jury, L.; Dosio, A.; Maraun, D.; Gutiérrez, J.M. Testing bias adjustment methods for regional climate change applications under observational uncertainty and resolution mismatch. *Atmos. Sci. Lett.* **2020**, *21*, e978. [[CrossRef](#)]
11. Themeßl, M.J.; Gobiet, A.; Leuprecht, A. Empirical statistical downscaling and error correction of daily precipitation from regional climate models. *Int. J. Climatol.* **2011**, *31*, 1530–1544. [[CrossRef](#)]
12. Silva, D.; Meza, F.J.; Varas, E. Estimating reference evapotranspiration (ET0) using numerical weather forecast data in central Chile. *J. Hydrol.* **2010**, *8*, 64–71. [[CrossRef](#)]
13. Tegos, A.; Efstratiadis, A.; Malamos, N.; Mamassis, N.; Koutsoyiannis, D. Evaluation of a parametric approach for estimating potential evapotranspiration across different climates. *Agric. Agric. Sci. Procedia* **2015**, *8*, 2–9.
14. Paredes, P.; Pereira, L.S.; Almorox, J.; Darouich, H. Reference grass evapotranspiration with reduced data sets: Parameterization of the FAO Penman-Monteith temperature approach and the Hargreaves-Samani equation using local climatic variables. *Agric. Water Manag.* **2020**, *240*, 106210. [[CrossRef](#)]
15. Chebil, A.; Kahil, T.; Oueslati, B. Policy measures for reducing aquifer depletion in a context of climate change: The case of the coastal area of Cap-Bon. *New Medit.* **2018**, *4*, 34–44. [[CrossRef](#)]
16. Maeda, E.E.; Wiberg, D.A.; Pellikka, P.K.E. Estimating reference evapotranspiration using remote sensing and empirical models in a region with limited ground data availability in Kenya. *Appl. Geogr.* **2011**, *31*, 251–258. [[CrossRef](#)]
17. Lasram, A.; Dellagi, H.; Dessalegn, B.; Dhehibi, B.; Ben Mechlia, N. Farmers' willingness to adapt to climate change for sustainable water resources management: A case study of Tunisia. *J. Water Clim. Change* **2018**, *9*, 598–610. [[CrossRef](#)]
18. Li, C.; Wu, P.T.; Li, X.L.; Zhou, T.W.; Sun, S.K.; Wang, Y.B.; Luan, X.B.; Yu, X. Spatial and temporal evolution of climatic factors and its impacts on potential evapotranspiration in Loess Plateau of Northern Shaanxi, China. *Sci. Total Environ.* **2017**, *589*, 165–172. [[CrossRef](#)]
19. Nam, W.H.; Hong, E.M.; Choi, J.Y. Assessment of water delivery efficiency in irrigation canals using performance indicators. *Irrig. Sci.* **2016**, *34*, 129–143. [[CrossRef](#)]
20. Tabari, H.; Marofi, S.; Aeini, A.; Hosseinzadeh Talaei, P.; Mohammadi, K. Trend analysis of reference evapotranspiration in the western half of Iran. *Agric. For. Meteorol.* **2011**, *151*, 128–136. [[CrossRef](#)]
21. Rahman, M.A.; Yunsheng, L.; Sultana, N.; Ongoma, V. Analysis of reference evapotranspiration (ET0) trends under climate change in Bangladesh using observed and CMIP5 data sets. *Meteorol. Atmos. Phys.* **2018**, *131*, 639–655. [[CrossRef](#)]
22. Chaouche, K.; Neppel, L.; Dieulin, C.; Pujol, N.; Ladouche, B.; Martin, E.; Salas, D.; Caballero, Y. Analyses of precipitation, temperature and evapotranspiration in a French Mediterranean region in the context of climate change. *Comptes Rendus Geosci.* **2010**, *342*, 234–243. [[CrossRef](#)]
23. Yassena, A.N.; Nama, W.H.; Honge, E.M. Impact of climate change on reference evapotranspiration in Egypt. *Catena* **2020**, *194*, 104711. [[CrossRef](#)]
24. Sáenz de la Torre, J.J.; Suárez, E.; Iglesias, D.; Sánchez, I.; Pérez, A.; Tuní, M.; García, M.; San-Martín, D.; Iturbide, M.; Gutiérrez, J.M. Climadjust: Easing the Bias Adjustment process through a user-friendly web service. In Proceedings of the EGU General Assembly, Online, 19–30 April 2021. [[CrossRef](#)]
25. Cutillas-Lozano, L.G.; Cruz López, M.S.; Pérez Velasco, A.; Andrés-Doménech, I.; Olcina-Cantos, J. Local-scale regionalisation of climate change effects on rainfall pattern: Application to Alicante City (Spain). *Theor. Appl. Climatol.* **2023**, *154*, 377–402. [[CrossRef](#)]
26. D'Oria, M.; Ferraresi, M.; Tanda, M.G. Historical trends and high-resolution future climate projections in northern Tuscany (Italy). *J. Hydrol.* **2017**, *555*, 708–723. [[CrossRef](#)]
27. Peres, D.J.; Senatore, A.; Nanni, P.; Cancelliere, A.; Mendicino, G.; Bonaccorso, B. Evaluation of EURO-CORDEX (Coordinated Regional Climate Downscaling Experiment for the Euro-Mediterranean area) historical simulations by high-quality observational datasets in southern Italy: Insights on drought assessment. *Nat. Hazards Earth Syst. Sci.* **2020**, *20*, 3057–3082. [[CrossRef](#)]
28. Lange, S. Trend-preserving bias adjustment and statistical downscaling with ISIMIP3BASD (v1.0). *Geosci. Model Dev.* **2019**, *12*, 3055–3070. [[CrossRef](#)]
29. Cannon, A.J.; Sobie, S.R.; Murdock, T.Q. Bias Correction of GCM Precipitation by Quantile Mapping: How Well Do Methods Preserve Changes in Quantiles and Extremes? *J. Clim.* **2015**, *28*, 6938–6959. [[CrossRef](#)]
30. Tegegne, G.; Melesse, A.M. Comparison of Trend Preserving Statistical Downscaling Algorithms Toward an Improved Precipitation Extremes Projection in the Headwaters of Blue Nile River in Ethiopia. *Environ. Process.* **2021**, *8*, 59–75. [[CrossRef](#)]
31. Hargreaves, G.H.; Samani, Z.A. Reference crop evapotranspiration from temperature. *Appl. Eng. Agric.* **1985**, *1*, 96–99. [[CrossRef](#)]

32. Raziei, T.; Pereira, L.S. Estimation of ETo with Hargreaves–Samani and FAO-PM temperature methods for a wide range of climates in Iran. *Agric. Water Manag.* **2013**, *121*, 1–18. [[CrossRef](#)]
33. Sabziparvar, A.A.; Tabari, H. Regional Estimation of Reference Evapotranspiration in Arid and Semiarid Regions. *J. Irrig. Drain. Eng.* **2010**, *136*, 724–731. [[CrossRef](#)]
34. Jabloun, M.; Sahli, A. Evaluation of FAO-56 methodology for estimating reference evapotranspiration using limited climatic data: Application to Tunisia. *Agric. Water Manag.* **2008**, *95*, 707–715. [[CrossRef](#)]
35. Yu, P.S.; Yang, T.C.; Wu, C.K. Impact of climate change on water resources in southern Taiwan. *J. Hydrol.* **2002**, *260*, 161–175. [[CrossRef](#)]
36. Thiel, H. A Rank-Invariant Method of Linear and Polynomial Regression Analysis. Part 3. *Proc. Koninklijke Ned. Akad. Van Wetenschappen A* **1950**, *53*, 1397–1412.
37. Sen, P.K. Estimates of the regression coefficient based on Kendall's tau. *J. Am. Stat. Assoc.* **1968**, *63*, 1379–1389. [[CrossRef](#)]
38. Latrech, B.; Yacoubi, S.; Hermassi, T.; Slatni, A.; Jarray, F.; Pouget, L. Homogeneity and Trend Analysis of Climatic Variables in Cap-Bon Region of Tunisia. *Appl. Sci.* **2023**, *13*, 10593. [[CrossRef](#)]
39. Taylor, K.E. Summarizing multiple aspects of model performance in a single diagram. *J. Geophys. Res.* **2001**, *106*, 7183–7192. [[CrossRef](#)]
40. Gado, T.A.; Mohameden, M.B.; Rashwan, I.M.H. Bias correction of regional climate model simulations for the impact assessment of the climate change in Egypt. *Environ. Sci. Pollut. Res.* **2021**, *29*, 20200–20220. [[CrossRef](#)]
41. Alexandaris, S.; Stricevic, R.; Petkovic, S. Comparative analysis of reference evapotranspiration from the surface of rainfed grass in central Serbia calculated by six empirical methods against the Penman-Monteith formula. *Eur. Water* **2008**, *21*, 17–28.
42. Senatore, A.; Fuoco, D.; Maiolo, M.; Mendicino, G.; Smiatek, G.; Kunstmann, H. Evaluating the uncertainty of climate model structure and bias correction on the hydrological impact of projected climate change in a Mediterranean catchment. *J. Hydrol. Reg. Stud.* **2022**, *42*, 101120. [[CrossRef](#)]
43. Sellami, H.; Benabdallah, S.; La Jeunesse, I.; Vanclooster, M. Quantifying hydrological responses of small Mediterranean catchments under climate change projections. *Sci. Total Environ.* **2016**, *543*, 924–936. [[CrossRef](#)]
44. Sundaram, G.; Radhakrishnan, S. Assessment of various bias correction methods and future projection of minimum and maximum temperatures using regional climate model over Thanjavur district. *Arab. J. Geosci.* **2022**, *15*, 1162. [[CrossRef](#)]
45. Tabari, H.; Hosseinzadeh Talaei, P. Recent trends of mean maximum and minimum air temperatures in the western half of Iran. *Meteorol. Atmos. Phys.* **2011**, *111*, 121–131. [[CrossRef](#)]
46. Lin, P.; He, Z.; Du, J.; Chen, L.; Zhu, X.; Li, J. Impacts of climate change on reference evapotranspiration in the Qilian Mountains of China: Historical trends and projected changes. *Int. J. Climatol.* **2018**, *38*, 2980–2993. [[CrossRef](#)]
47. Zhao, J.; Xia, H.; Yue, Q.; Wang, Z. Spatiotemporal variation in reference evapotranspiration and its contributing climatic factors in China under future scenarios. *Int. J. Climatol.* **2023**, *40*, 3813–3831. [[CrossRef](#)]

**Disclaimer/Publisher's Note:** The statements, opinions and data contained in all publications are solely those of the individual author(s) and contributor(s) and not of MDPI and/or the editor(s). MDPI and/or the editor(s) disclaim responsibility for any injury to people or property resulting from any ideas, methods, instructions or products referred to in the content.